Nano Research

ISSN 1998-0124 CN 11-5974/O4
https://doi.org/10.1007/s12274-022-4433-0

Research Article

Interfacial synergistic effect in SnO_2/PtNi nanocrystals enclosed by high-index facets for high-efficiency ethylene glycol electrooxidation

Shuna Li[1,§], Haixiao Sun[1,§], Jiaai Zhang[1], Longjiao Zheng[1], Yunrui Li[1], Xu Fang[1], Yujie Liu[1], Qi Song[1], Zhen Wang[1], Yufeng Gao[1], Xin Zhang[1] (✉), Xiaoping Dai[1], Yandi Cai[2], and Fei Gao[2] (✉)

[1] *State Key Laboratory of Heavy Oil Processing, College of Chemical Engineering and Environment, China University of Petroleum, Beijing 102249, China*

[2] *Jiangsu Key Laboratory of Vehicle Emissions Control, School of the Environment, Nanjing University, Nanjing 210093, China*

[§] *Shuna Li and Haixiao Sun contributed equally to this work.*

Received: 22 February 2022 / **Revised:** 29 March 2022 / **Accepted:** 14 April 2022

ABSTRACT

Strengthening the oxide–metal interfacial synergistic interaction in nanocatalysts is identified as potential strategy to boost intrinsic activities and the availability of active sites by regulating the surface/interface environment of catalysts. Herein, the SnO_2/PtNi concave nanocubes (CNCs) enclosed by high-index facets (HIFs) with tunable SnO_2 composition are successfully fabricated through combining the hydrothermal and self-assembly method. The interfacial interaction between ultrafine SnO_2 nanoparticles and PtNi with HIFs surface structure is characterized by analytical techniques. The as-prepared 0.20%SnO_2/PtNi catalyst exhibits extraordinarily high catalytic performance for ethylene glycol electrooxidation (EGOR) in acidic conditions with specific activity of 3.06 mA/cm^2, which represents 6.2-fold enhancement compared with the state-of-the-art Pt/C catalyst. Additionally, the kinetic study demonstrates that the strong interfacial interaction between SnO_2 and PtNi not only degrades the activation energy barrier during the process of EGOR but also enhances the CO-resistance ability and long-term stability. This study provides a novel perspective to construct highly efficient and stable electrocatalysts for energy conversions.

KEYWORDS

Pt-based catalyst, high-index facets, undercoordinated surface atoms, interfacial synergistic effect, ethylene glycol electrooxidation

1 Introduction

The platinum-based nanocrystals enclosed by high-indexed facets (HIFs) feature more coordination unsaturated atoms and abundant active sites than those of catalysts with low-indexed facets, which are regarded as the prospective catalysts to replace the state-of-the-art Pt/C catalyst in field of electrochemical reactions, including small organic molecules electrooxidation reaction, water splitting, and oxygen reduction reaction (ORR) [1–3]. The direct alcohols fuel cells (DAFCs), as renewable conversion devices, possess high-efficient transformation of chemical energy (e.g., methanol, ethanol, and ethylene glycol) into electronic energy, which have captured extensive attention owing to high power density and environment friendliness. The ethylene glycol molecules possess less toxicity, volatility, and long chain structure in comparison with methanol, which can impede the damage of electrolyte membranes [4]. Therefore, it is greatly significant to construct the ethylene glycol fuel cells for extending the life of the electrolyte membranes. For ethylene glycol electrooxidation (EGOR) reaction, the Pt based catalysts with HIFs not only facilitate for the oxidation of intermediate adsorbed CO (CO_{ads}) but also promote the scission of C–C bond during the process of electrooxidation [5]. Nevertheless, the HIFs with high surface energy are usually metastable in thermodynamics, thus leading to the reconstruction of surface atom during the process of long-term stability tests in electrochemical energy conversion, particularly for the catalysts with unique morphologies. For unstable HIFs structure, it can give rise to the migration and aggregation of surface atoms during the process of reaction and thereby producing significant effects on atomic arrangement, catalytic performance, and longevity of nanocrystals [6–8]. It is thus crucial to explore an effective strategy to stabilize the surface structure of HIFs, while also help maintain high catalytic activity and durability during the process of electrocatalysis.

Usually, great efforts have been devoted to constructing stable structured catalysts to enhance the intrinsic activity and durability by tailoring surface electronic/geometry structure of nanocrystals [9]. For supported catalysts, the Pt-based alloy enclosed by HIFs was embedded into porous graphene or nickel hydroxide to display improved hydrogen evolution reaction performance in alkaline media [10, 11]. Our group has initially proposed a novel strategy by engineering the stable and high catalytic activity of electro-catalytic catalysts by implanting non-noble metal or nonmetals as "active auxiliaries" into the Pt based metal nanocrystals with HIFs. The strategy has been proved by using the

Address correspondence to Xin Zhang, zhangxin@cup.edu.cn; Fei Gao, gaofei@niu.edu.cn

metals (Mo or Ga) as active auxiliaries implanted onto the surface of Pt_3Mn exposed with HIFs to reach high electrocatalytic activity and stability for alcohols oxidation reaction [5, 12]. The metal oxide as active additive has attracted considerable attentions in enhancement catalytic performance in comparison with other materials, which is attributed to interfacial effects via increasing contact area between oxide and metals. Taking into account that the oxide-on-metal catalysts can regulate coordination environment and surface electronic structure by interfacial synergistic effect, thereby influencing catalytic properties [13, 14], we thus envisaged that by implanting metal oxide as "an active auxiliary" into the near-surface of noble metal nanocrystals exposed with HIFs to engineer a stable structured catalyst. For instance, Xie and co-workers [15] reported that the inverse RuO_2/Pd catalyst exhibited extraordinary ORR performance and presented attenuation of only 25.6% initial mass activity after 20,000 cycles. The amplified interface effect between RuO_2 and Pd nanosheets accounts for the enhanced catalytic performance and durability. Therefore, the oxide-metal catalysts exposed with HIFs offer new inspirations for designing efficient and stable supported electrocatalyst by strengthening the interfacial effect. Given the several dozens of papers now published on metal oxide modified noble metal nanocrystals with low-index facets, no attempt has been tried for noble metal nanocrystals bounded with HIFs modified by implanting metal oxide as "an active auxiliary".

Compared with other metal oxide materials, tin oxide (SnO_2) offers significant advantage for adsorption and dissociation of H_2O as well as oxidation and elimination of intermediates CO_{ads} on the surface of catalysts during the process of electrooxidation. The interfacial effect and bifunctional mechanism between SnO_2 and support materials can enhance the electrooxidation properties [16–18]. For example, Sun and co-workers documented that the synergistic effect between ordered Pt_3Sn and SnO_2 could enhance the catalytic activity, stability, and anti-poisoning ability for methanol and ethanol oxidation reactions [16]. Regarding interfacial effect, the various degrees of interfacial contact impose a profound effect on catalytic properties [17]. Wang's group found that PdSn alloys are closely contacted with SnO_2 to generate massive active sites (interfacial contact), which accounts for excellent catalytic performance for formic acid oxidation and high CO_{ads} tolerance in PdSn-SnO_2-islands/C catalyst. Moreover, the dual-site cascade mechanism occurred on the SnO_x/Pt-Cu-Ni heterojunction structure during the process of ORR. The former two steps take place on SnO_x sites (*OOH and *O generation) and the remaining steps occur at adjacent Pt sites to facilitate the ORR performance [18]. It should be emphasized that although the decoration of SnO_2 is an effective approach for improving electrocatalytic properties, few literatures have been studied regarding the modification and stabilization the HIF structure of catalysts via oxide-metal interfacial synergism effect. It is therefore of great significance for construction the catalysts which oxides modified the structure of HIF to elevate catalytic properties by interfacial synergistic effect.

Inspired by this, the SnO_2/PtNi catalysts enclosed by HIFs are designed and synthesized by integrating hydrothermal and self-assembly methods, as illustrated in Scheme 1. Afterwards, the experimental and characterization technologies are employed to investigate the interfacial effect and the relationship of structure-performance of catalysts towards EGOR. The SnO_2/PtNi catalysts display the enhancement of catalytic activity, long-term durability, and CO_{ads} anti-poisoning for EGOR in comparison to PtNi concave nanocubes (CNCs) and commercial Pt/C. Particularly, the 0.20%SnO_2/PtNi catalyst exhibits the highest activity and durability as well as the oxidation of intermediates of CO_{ads}, which is attributed to synergistic effect and optimized interfacial contact between SnO_2 and PtNi CNCs. Moreover, the experimental results indicate that the low reaction activation energy during the process of EGOR derives from the synergistic catalytic effect in 0.20%SnO_2/PtNi catalyst.

2 Experimental

2.1 Synthesis of PtNi CNCs

38 mg of glycine and 220 mg of polyvinyl pyrrolidone (PVP) were mixed with the aqueous solution containing 1 mL H_2PtCl_6 (20 mM) and 4 mL $NiCl_2$ (1.66 mM). After stirred and sonicated for 5 min, the homogeneous solution was transferred into 20 mL Teflon-lined stainless-steel autoclave and heated to 200 °C for 6 h under sealed conditions. Then, the obtained products were washed and centrifuged several times by the mixture solution of water and ethanol.

2.2 Synthesis of ultrasmall SnO_2 nanoparticles (NPs)

1 g $SnCl_4$ was dissolved into mixed solution including 50 mL distilled water and 0.5 g triethylenediamine (TEDA), and then stirred for 30 min. Afterwards, the resulting solution was transferred into 100 mL Teflon-lined stainless-steel autoclave and maintained at 110 °C for approximately 40 h. The final products were washed and centrifuged by water and ethanol.

2.3 Synthesis of SnO_2/PtNi catalyst with adjustable SnO_2 loading

First, the PtNi CNCs were dispersed into 8 mL ethanol, then 4 mL of aqueous solution consisting of 80 mg PVP was injected into above solution and the mixture was stirred for 24 h. The obtained

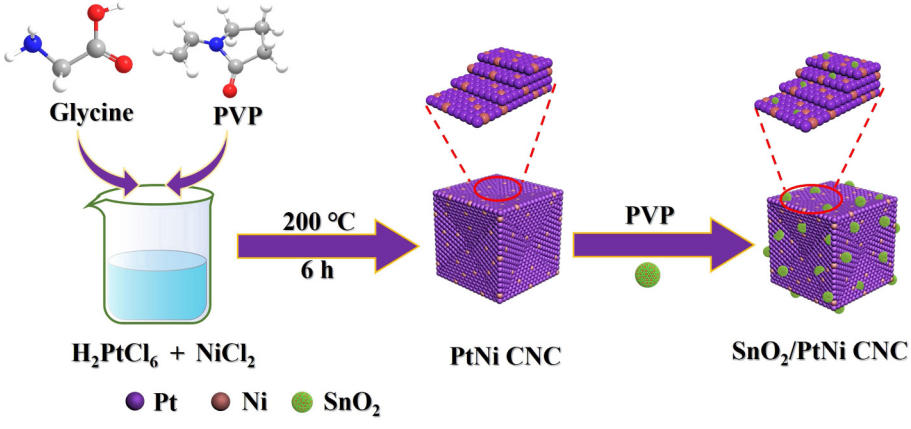

Scheme 1 Illustration of the preparation of SnO_2/PtNi catalysts.

homogeneous solution was centrifuged several times and dispersed into 8 mL water. Subsequently, 3 mL ethanol solution including SnO_2 composition (30, 70, and 134 μg) was dropped into the PVP-PtNi CNCs solution one by one. The mixture was stirred for 24 h, and washed and centrifuged with ethanol/deionized water mixture (volume ratio of 1/1), then freeze-dried at −50 °C. The obtained catalysts were $x$$SnO_2$/PtNi, where x refers to the weight fraction of SnO_2.

2.4 Electrochemical measurements

Ethylene glycol electro-oxidation experiments were carried out on CHI 760E electrochemistry workstation. The glassy carbon electrode (GCE, 3 nm in diameter), saturated calomel electrode (SCE), and the carbon rod were selected as the working, reference, and counter electrodes, respectively. Before the experiments, the GCE was consecutively polished by different aluminum oxide power (0.3 and 0.05 μm Al_2O_3). Then, the catalysts ink containing 6 μg catalyst was dropped onto the surface of GCE. In order to remove the capping agents, the electrodes were treated under ultraviolet (UV) lamp for overnight before the electrochemical test. Successively, 2 μL of 0.05 wt.% Nafion in ethanol was covered on the surface of electrodes and dried under infrared (IR) lamp. The cyclic voltammetry (CV) measurements were performed to estimate the electrochemical active surface area (ECSA) in N_2-saturated 0.1 M $HClO_4$ electrolyte at the range of −0.26–0.70 V (vs. SCE) with a sweep rate of 50 mV/s. The ECSA values were calculated by measuring the underpotential deposited hydrogen (H_{upd}) area. The ethylene glycol electro-chemical oxidation reaction was conducted in mixed solution of 0.1 M $HClO_4$ and 0.5 M ethylene glycol (N_2-saturated) with the potential scanned from −0.26 to 0.94 V (SCE) at a scan rate of 50 mV/s. The stability and long-term durability of catalysts were evaluated by chronoamperometry at 0.4 V (vs. SCE) and consecutive CV cycles in 0.1 M $HClO_4$ solution containing 0.5 M ethylene glycol, respectively. With regarding to CO stripping tests, the electrode with loaded catalyst was immersed into 0.1 M $HClO_4$ electrolyte with CO for a certain time. The non-adsorbed CO species in solution was removed by bubbling N_2. The potential (E_{SCE}) was converted to the reversible hydrogen electrode (E_{RHE}) based on equation: $E_{RHE} = E_{SCE} + 0.0591\ pH + 0.24\ V$.

3 Results and discussion

3.1 Catalyst characterization

The morphology and structure of as-prepared PtNi CNCs and SnO_2/PtNi catalysts with different SnO_2 loading were manifested by transmission electron microscopy (TEM), as illustrated in Fig. 1, and Figs. S4 and S5 in the Electronic Supplementary Material (ESM). As it can be seen from Figs. 1(a)–1(c), the PtNi alloys are endowed with concave structure with an average apex-to-apex length of 37.2 ± 5.8 nm. Based on the [001] direction of selected area electron diffraction (SAED) (Fig. 1(d)), the angles between crystal facets of PtNi were measured to be approximately 9.5°, 11.3°, 14.0°, and 15.9°, which were just in coincidence with {610}, {510}, {410}, and {720} high-index facets of Pt (Figs. S1 and S2 in the ESM), respectively [19, 20]. The result demonstrates the formation of HIFs on the surface of PtNi CNCs. Notably, the interplanar fringe spacing in corresponding high-resolution TEM (HRTEM) image (Fig. 1(e)) is ca. 0.199 nm, which is associated with the (200) facet of face-centered cubic (fcc) Pt [21]. The elemental mapping of PtNi CNCs suggests that the Pt and Ni elements are evenly dispersed across the nanoparticles. Moreover, the SAED pattern of PtNi CNCs (Fig. 1(f)) shows diffraction rings that correspond to (100) and (110) facets. The SnO_2/PtNi catalysts with different SnO_2 composition were prepared via self-assembly process. As shown in Fig. S3 in the ESM, the obtained SnO_2 nanoparticles are spherical with an average diameter 3.0 ± 0.5 nm, which is ascribed to the stabilization and coordinative saturation of TEDA molecules during the hydrothermal reaction [22]. The TEM images of 0.08%SnO_2/PtNi, 0.20%SnO_2/PtNi, and 0.35%SnO_2/PtNi CNCs are illustrated in Figs. 1(g)–1(k), and Figs. S4 and S5 in the ESM, respectively. The average lengths of 0.08%SnO_2/PtNi, 0.20%SnO_2/PtNi, and 0.35%SnO_2/PtNi CNCs are measured to be 38.6 ± 4.3, 41.2 ± 6.8, and 48.2 ± 6.5 nm, respectively. The results show that the average size of nano-cubic increases with the addition of SnO_2 composition, which in turn proves the successful preparation of catalyst. For 0.20%SnO_2/PtNi catalyst, every PtNi CNC is closely surrounded by multiple tiny SnO_2 NPs, indicating the formation of interface between SnO_2 and PtNi CNCs, as shown in Fig. 1(i). For 0.35%SnO_2/PtNi, massive SnO_2 NPs are accumulated and occupied on the surface of PtNi to form larger particle, thereby reducing the exposure of interfacial active sites (Figs. S5(a)–S5(c) in the ESM). For 0.20%SnO_2/PtNi catalyst, the apparent lattice fringe with spacing of 0.203 nm is associated with Pt (200) facet, while the interplanar spacings about 0.174, 0.234, and 0.338 nm agreed with (211), (200), and (110) planes of SnO_2, respectively. The result corroborates the presence of SnO_2 and the successful modification of SnO_2 on PtNi [23, 24]. As shown in Figs. 1(i_3) and 1(i_4), there is an obvious interfacial region of lattice fringes between PtNi and SnO_2, which gives rise to the interfacial synergy effect to facilitate the electron transfer and catalytic performance for EGOR [25, 26]. From the results of facets angle calculations, the morphology of concave nano-cubic and surface structure of HIFs can be retained after the decoration with different SnO_2 loading (Fig. S6 in the ESM). Both Sn and O elements are distributed homogeneously throughout the entire nanoparticles in SnO_2/PtNi catalysts with different SnO_2 (Fig. 1(k), and Figs. S4(e) and S5(f) in the ESM), which confirms the successful decoration of SnO_2.

The crystalline structure of as-fabricated SnO_2, PtNi, and SnO_2/PtNi catalysts with different SnO_2 composition has been characterized by the X-ray diffraction (XRD). As presented in Fig. S7(a) in the ESM, the distinctive diffraction peaks positions at 26.6°, 33.5°, 38.3°, 51.8°, and 64.9° are associated with (110), (101), (111), (211), and (112) planes of SnO_2 (JCPDS No. 41-1445), respectively [22, 25, 27]. The broad diffraction peaks suggest SnO_2 NPs with smaller size, which is in accordance with HRTEM observation. Additionally, there is no obviously diffraction peak of SnO_2 on SnO_2/PtNi catalyst owing to the smaller size or the low loading of SnO_2. As shown in Fig. 2(a), the diffraction peaks of PtNi and SnO_2/PtNi catalysts are attributed to (111), (200), (220), and (311) planes [28]. Compared with pure fcc Pt (JCPDS No. 04-0802), the diffraction peaks positively shift indicating that the lattice strain results from the incorporation of Ni into Pt in PtNi CNC catalyst [29]. The SnO_2/PtNi catalysts with different SnO_2 decoration showed different degrees of negatively shift compared to PtNi, suggesting that the lattice fringe of Pt was modified after SnO_2 decoration (Fig. S7(b) and Table S2 in the ESM), which is consistent with the result of HRTEM. X-ray photoelectron spectroscopy (XPS) was applied to investigate the surface chemical states, surface composition, and electron interaction among various elements of as-prepared catalysts. The XPS survey spectra confirm the coexistence of Pt, Ni, Sn, and O elements in catalysts (Fig. S7(c) in the ESM), which is in accordance with the above element mapping results. As indicated in Fig. 2(b), the XPS spectra of Pt 4f can be deconvoluted into two group peaks corresponding to metallic Pt^0 and oxidized species of Pt^{2+}. The metallic state of Pt accounts for the vast majority in surface structure, whereas only a small proportion of Pt with oxidized state originates from the Pt-

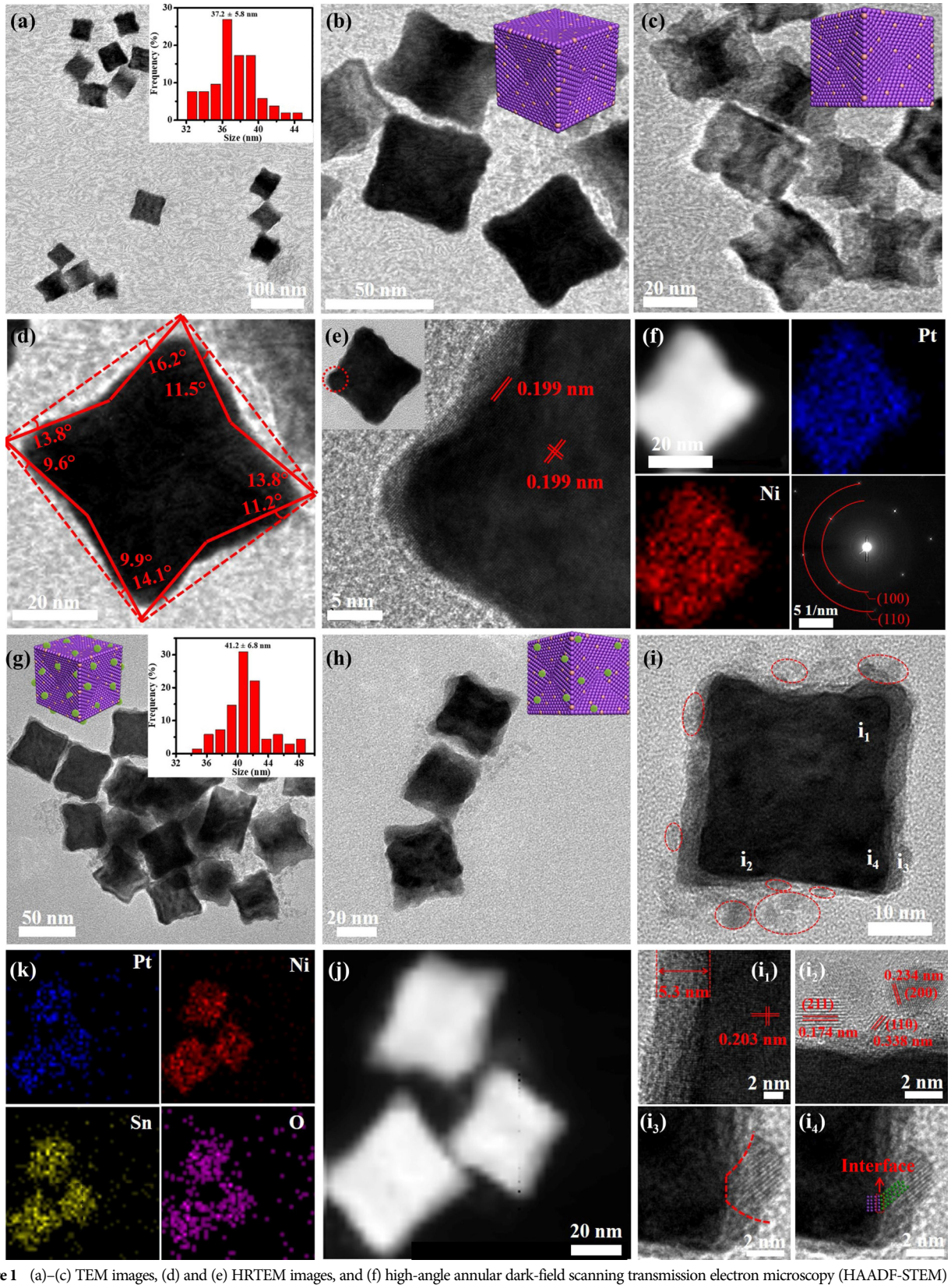

Figure 1 (a)–(c) TEM images, (d) and (e) HRTEM images, and (f) high-angle annular dark-field scanning transmission electron microscopy (HAADF-STEM) image and the corresponding elemental mapping images of PtNi CNCs. (g)–(i) TEM images of 0.20%SnO_2/PtNi, (i_1) and (i_2) enlarged views of the catalyst edge, and (i_3) and (i_4) the interface of SnO_2 and PtNi. (j) HAADF-STEM image and (k) the corresponding elemental mapping images of 0.20%SnO_2/PtNi catalyst.

O layer. For PtNi catalyst, the peak at 70.21 eV shows negative shift of 0.69 eV in comparison to pure metallic Pt (70.90 eV), indicating that the incorporation of Ni into Pt can modify the electronic structure [30].

For SnO_2/PtNi with different SnO_2 composition, the binding energy of Pt $4f_{7/2}$ is up-shift about 0.28, 0.29, and 0.06 eV, revealing that the electrons transfer between Pt and the interface SnO_2/PtNi [15]. For XPS spectra of Ni 2p, the signal is quite weaker in SnO_2/PtNi than that of PtNi catalyst, which is attributed to the coverage of SnO_2 on the surface of PtNi. Additionally, the Sn 3d peaks are deconvoluted into two symmetrical peaks at about 486.57 and 495.02 eV in SnO_2/PtNi catalysts with different SnO_2 composition corresponding to the Sn^{4+} $3d_{5/2}$ and Sn^{4+} $3d_{3/2}$ of SnO_2, respectively [31, 32]. In contrast, the binding energy of Sn $3d_{5/2}$

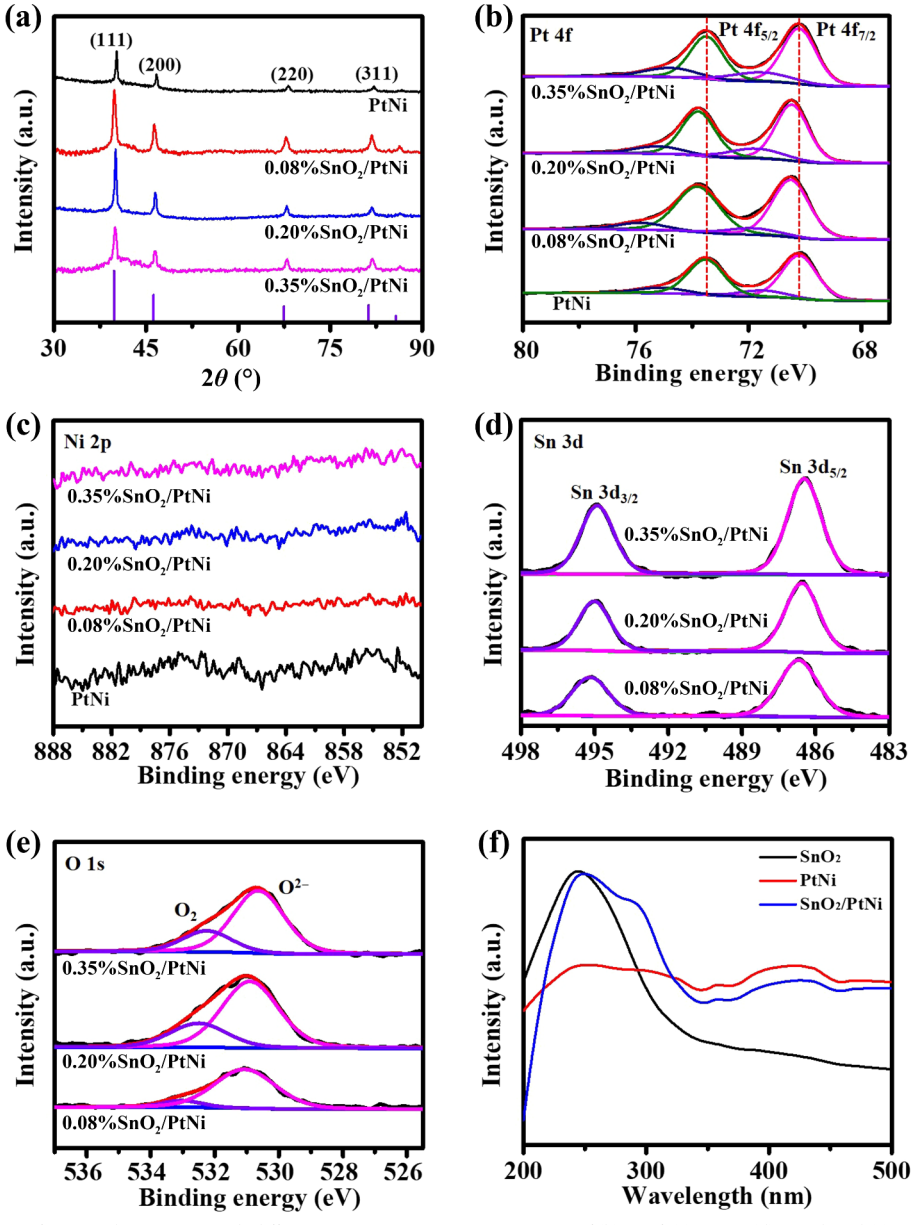

Figure 2 (a) XRD patterns of PtNi and SnO_2/PtNi with different SnO_2 composition. XPS spectra of (b) Pt 4f, (c) Ni 2p, (d) Sn 3d, and (e) O 1s in as-prepared catalyst. (f) UV–vis adsorption spectra of SnO_2, PtNi, and SnO_2/PtNi catalysts.

peaks in 0.08%SnO_2/PtNi (486.69 eV), 0.20%SnO_2/PtNi (486.57 eV), and 0.35%SnO_2/PtNi (486.46 eV) was slightly shifted to lower energy than the pure SnO_2 (487.3 eV), suggesting that the interfacial interaction and electronic transfer exist in SnO_2 and PtNi [33]. Besides, the O 1s peaks are observed at the positions of 531.2 and 532.9 eV (Fig. 2(e)) attributable to the lattice oxygen (O^{2-}) and interfacial oxygen (O_2), respectively [25]. With the increment of SnO_2 composition, the content of interfacial oxygen (O_2) shows growing tendency, implying the formation of interfacial interactions between PtNi and SnO_2 from the electrons transfer, as shown in Fig. S8 in the ESM. In order to further confirm the interfacial interaction, the ultraviolet–visible (UV–vis) adsorption spectra of SnO_2, PtNi, and SnO_2/PtNi catalysts are recorded in Fig. 2(f). Notably, the SnO_2 NPs, PtNi CNCs, and SnO_2/PtNi catalyst possess distinguishable adsorption peaks occurring in the region of 200–500 nm. As illustrated in Fig. 2(f), the strong adsorption peak of SnO_2 NPs is located around at 243 nm, while the broad adsorption peaks ranging from 200 to 300 nm are ascribed to PtNi [34–36]. For SnO_2/PtNi catalyst, it can be found the corresponding adsorption peaks are slightly red shifted to 250 and 293 nm, which is assigned to the interfacial electron coupling and transferring as well as strong interaction between SnO_2 and PtNi [35, 36].

3.2 Electrochemical performance

In order to systematically evaluate the correlation of electrocatalytic properties with structure, the PtNi CNCs and SnO_2/PtNi catalysts with different SnO_2 composition were explored as electrocatalysts towards EGOR, and then compared with commercial Pt/C in catalytic activity, durability, and CO_{ads} anti-poisoning ability. As shown in Fig. 3(a), the CVs were carried out in N_2-saturated 0.1 M $HClO_4$ electrolyte to measure the ECSA which was a significant parameter to assess the catalytic property on basis of the hydrogen adsorption/desorption regions. From Table S3 in the ESM, it is noticeable that the 0.20%SnO_2/PtNi catalyst exhibits an ECSA value of 22.2 m^2/g, which is much larger than those of 0.08%SnO_2/PtNi (14.8 m^2/g), 0.35%SnO_2/PtNi (7.4 m^2/g), and PtNi (6.6 m^2/g). For SnO_2/PtNi catalyst, the presence of SnO_2 can inhibit the Pt atom migration and aggregation and the passivation of Pt sites deriving from the adsorption of hydroxyl group [5]. Therefore, the SnO_2/PtNi with different SnO_2 loading exhibited larger ECSA values in

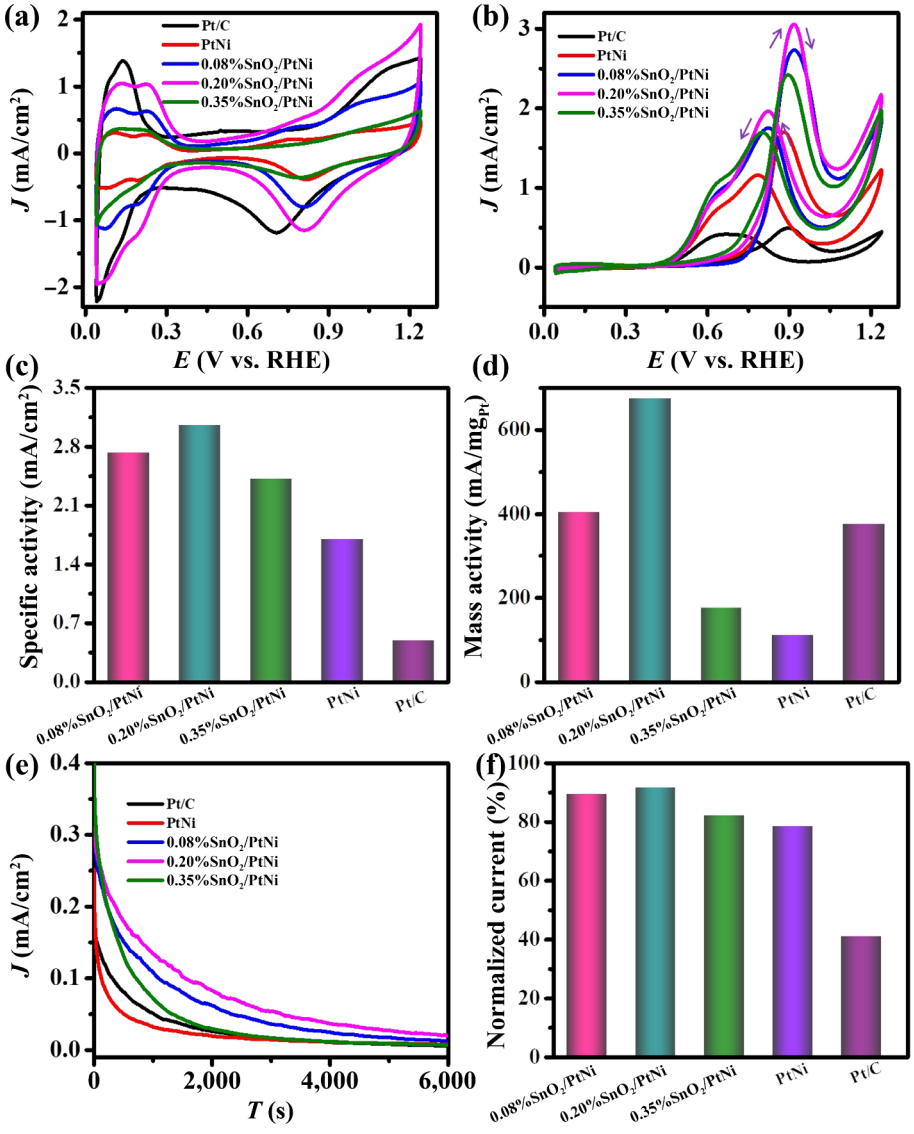

Figure 3 The cyclic curves of PtNi, 0.08%SnO_2/PtNi, 0.20%SnO_2/PtNi, 0.35%SnO_2/PtNi, and Pt/C catalysts in (a) 0.1 M $HClO_4$ solution and (b) 0.1 M $HClO_4$ with 0.5 M EG solution at scan of 50 mV/s. (c) The specific activity and (d) mass activity of different catalysts. (e) Current–time curves recorded at 0.7 V vs. RHE and (f) the durability comparison of as-prepared catalysts and Pt/C after 1,000 cycles.

comparison with PtNi catalyst. The result indicates that the 0.20%SnO_2/PtNi catalyst with larger ECSA allows for providing more catalytically active sites and enhances intrinsic activity towards EGOR, owing to the optimized interfacial synergistic interaction between ultra-small SnO_2 NPs and PtNi CNCs. The electrocatalytic activity of as-prepared catalysts and commercial Pt/C was examined in 0.1 M $HClO_4$ electrolyte containing 0.5 M EG with a sweep of 50 mV/s, as shown in Fig. 3(b). Two distinct peaks are clearly observed in the process of EGOR. The stronger oxidation peak in positive scan is ascribed to the oxidation of EG, while the weaker peak from negative sweep is corresponding to the removal of carbonaceous intermediates [37]. Figure 3(c) shows that the specific activities of 0.08%SnO_2/PtNi, 0.20%SnO_2/PtNi, and 0.35%SnO_2/PtNi are 2.73, 3.06, and 2.42 mA/cm^2, which are 1.61, 1.80, and 1.42 times than that of PtNi catalysts (1.70 mA/cm^2), respectively. Specifically, the optimal 0.20%SnO_2/PtNi achieves high specific activity, exceeding that of commercial Pt/C by 6.2 times. Meanwhile, the 0.20%SnO_2/PtNi catalyst also exhibits excellent mass activity of 675 mA/mg_{Pt}, which is superior than that of PtNi (112 mA/mg_{Pt}), indicating that the optimized interfacial synergistic effect is conductive to enhance the catalytic performance. The results of catalytic activity are consistent with ECSA trendy. The 0.20%SnO_2/PtNi catalyst displays exceptional specific and mass activities originating from the following aspects. Firstly, the presence of SnO_2 NPs is conductive to the adsorption and dissociation of H_2O, thus providing the sites of adsorbed OH species and facilitating the oxidation/deposition of CO_{ads} intermediates on the surface of catalysts [16]. More importantly, the amplified synergetic effect between SnO_2 and PtNi can produce strong interaction, which further optimizes the electronic structure of Pt and enhances the electrocatalytic properties for EGOR [12, 25].

In addition to catalytic activity, the stability and long-term durability are considered as vital factors for assessing the catalysts in the practical application. The stability of as-made catalysts and Pt/C towards EGOR was evaluated by chronoamperometric measurements in 0.1 M $HClO_4$ with 0.5 M EG at 0.7 V vs. RHE. For different electrocatalysts, the current densities displayed the decline trend gradually as the continuous reaction (Fig. 3(e)) owing to the accumulation of poisoning intermediates. After 6,000 s, the 0.20%SnO_2/PtNi catalyst displayed the least decay of current density in comparison with other catalysts. Besides, the long-term durability of catalysts was further tested by applying consecutive potential cycles with a sweep of 50 mV/s in 0.1 M $HClO_4$ solution containing 0.5 M EG. As shown in Fig. 3(f), the 0.20%SnO_2/PtNi catalyst can remain 91.6% of its initial activity

after 1,000 cycles, much higher than those of PtNi (78.7%) and commercial Pt/C catalyst (41.2%), suggesting that the decoration of SnO_2 can greatly improve the durability of catalysts. The results indicated that the strong interaction resulting from interfacial effect between SnO_2 and PtNi can not only immobilize and stabilize the surface structure of HIFs but also further enhance durability of catalysts. More importantly, the decoration of SnO_2 on the surface of PtNi can prevent Pt agglomeration and passivation of Pt sites, thereby increasing the exposure of Pt active sites and improving the catalytic performance [5, 38]. Furthermore, the optimized 0.20%SnO_2/PtNi catalyst displays excellent catalytic performance and durability for EGOR, which is much better than previously reported electrocatalysts (Table S5 in the ESM).

During the process of alcohol electrooxidation, the strong affinity between intermediates CO_{ads} and Pt active sites can deactivate the catalysts, so the anti-poisoning ability of CO_{ads} is an important criterion to evaluate the catalytic performance of catalysts. The CO stripping experiments are carried out in N_2-saturated 0.1 M $HClO_4$ electrolyte to identify the anti-CO poisoning ability of catalysts, as shown in Fig. S9 in the ESM. The onset and peak potentials of CO oxidation on as-prepared catalysts and commercial Pt/C are displayed in Figs. 4(a) and 4(b), and Table S4 in the ESM. As shown in Fig. 4(a), the onset potential of CO oxidation on PtNi (0.638 V vs. RHE) located at more negative position about 89 mV than that of Pt/C (0.727 V vs. RHE), reflecting that the incorporation of Ni into the Pt lattice can cause alloy effect which allows the oxidation of CO at relative low potentials. Compared with PtNi CNCs, the 0.20%SnO_2/PtNi catalyst displays more negative onset potential of CO oxidation (0.580 V vs. RHE), which can be ascribed to the interfacial synergistic effect between SnO_2 and PtNi. Besides, the peak potential of 0.20%SnO_2/PtNi catalyst shows the negative shift of 40 mV compared with Pt/C (Fig. 4(b)). These results demonstrate that the addition of SnO_2 on the surface of PtNi is more favorable to expose more Pt active sites and remove the intermediate CO_{ads}, further enhance the tolerance of CO_{ads} poisoning [31, 39]. Moreover, the SnO_2/PtNi catalysts with adjustable SnO_2 loading show multi-peaks for CO oxidation while the commercial Pt/C suggests only one oxidation peak, indicating the formation of multi-active sites for CO oxidation on the surface of SnO_2/PtNi catalysts. To further confirm the reactivity and superior electrocatalytic performance for EGOR on as-prepared catalysts and Pt/C, the study of kinetic was performed at different reaction temperatures. As indicated in Fig. S10 in the ESM, it can be observed that the peak current densities became larger with the increment of reaction temperature. The apparent activation energy (E_a) is calculated via the Arrhenius formula, which is evaluated by the linear regression between the reciprocal of temperature versus the log value of current density (Figs. 4(c) and 4(d)) [20, 40]. The E_a values for EGOR on Pt/C, PtNi, 0.08%SnO_2/PtNi, 0.20%SnO_2/PtNi, and 0.35%SnO_2/PtNi catalysts are 36.1, 25.5, 23.3, 21.4, and 24.8 kJ/mol, respectively. The 0.20%SnO_2/PtNi displayed the lowest E_a value among all catalysts, suggesting that the addition of SnO_2 is conductive to efficient ethylene glycol activation and optimized EGOR kinetics as well as accounting for improvement of electrocatalytic activity. The results clearly implied that the strong interaction deriving from interfacial synergism effect between ultra-small SnO_2 and PtNi in 0.20%SnO_2/PtNi catalyst was prone to decreasing reaction activation energy and accelerating electrooxidation kinetics.

3.3 Structure–activity relationship of catalysts

In accordance with the above viewpoint of all experimental results, the exceptional catalytic activity, durability, and CO anti-poisoning ability of SnO_2/PtNi catalyst with different SnO_2 composition towards EGOR could be attributed to following several aspects. (i) The SnO_2/PtNi with HIFs exhibited enhanced catalytic properties in comparison to Pt/C catalyst, which is attributed to the undercoordinated surface atoms from HIFs resulting in exposure more Pt active sites [41–44]. (ii) The presence of SnO_2 at the surface of PtNi can inhibit the Pt atom migration and aggregation caused by dissolution of transition metal in electrolyte as well as the passivation of Pt sites deriving

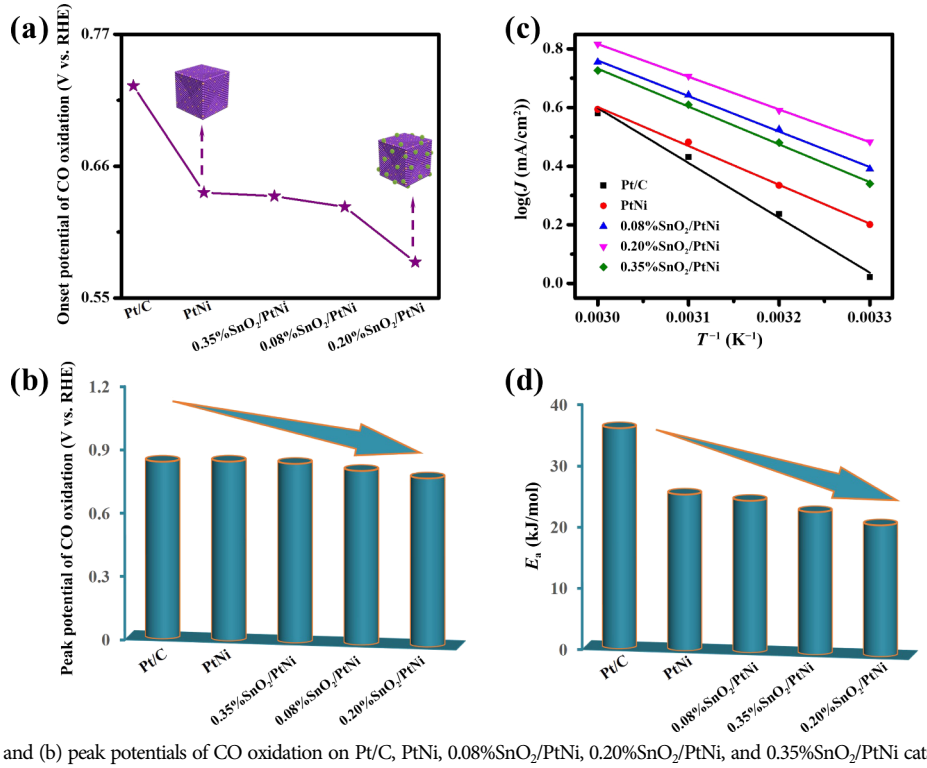

Figure 4 (a) The onset and (b) peak potentials of CO oxidation on Pt/C, PtNi, 0.08%SnO_2/PtNi, 0.20%SnO_2/PtNi, and 0.35%SnO_2/PtNi catalysts. (c) The Arrhenius curves and (d) the apparent activation energy of different catalysts.

from the adsorption of hydroxyl group [5, 39, 45]. (iii) The interactions from interfacial synergistic effect in SnO_2/PtNi can modify and stabilize the electronic structure of surface, and further ameliorate the stability and durability of catalyst [46, 47]. For EGOR, the SnO_2/PtNi showed two possible active sites including SnO_2 sites and Pt active sites. The 0.20%SnO_2/PtNi catalyst with optimal SnO_2 composition displays optimal distance between Pt active sites and SnO_2 NPs, which is favorable for the oxidation and detachment of CO_{ads} on the adjacent Pt active sites. When excessive SnO_2 is introduced in this system, the ultrafine SnO_2 is aggregated into larger particle on the surface of PtNi owing to high surface energy, as shown in Fig. S11 in the ESM. The more sufficient SnO_2 on the surface of PtNi may produce blockage effect or form stronger binding with adsorbed OH species to difficult release, which in turn affects the oxidation of CO and catalytic activity [45]. More importantly, the experimental kinetic result indicated that the 0.20%SnO_2/PtNi catalyst with optimized interface synergistic effect displayed lower activation energy barrier during the process of EGOR, which further accelerates the oxidation of ethylene glycol [48–50]. The previous literatures [51, 52] reported that the electrooxidation reaction of ethylene glycol involves complete oxidation and incomplete oxidation, the detailed pathway and electronic transfer process are illustrated in Fig. S12 in the ESM. The necessity of excess activation energies is used for the scission of C–C bond and C–H bond by delivering electrons in oxidation pathway to produce CO_2 and numerous of C2 species (glycolaldehyde, glyoxal, and glycolic acid) [53–55]. It is generally reported that the ability of anti-poisoning of CO_{ads} intermediates is key descriptor to estimate the catalytic property [56, 57]. Figure 5 showed the proposed schematic illustration of electrooxidation of ethylene glycol on SnO_2/PtNi catalyst interface. The modification of SnO_2 on the surface of PtNi produces the active interface which accounts for the superior catalytic performance by strong interaction from interfacial synergistic effect.

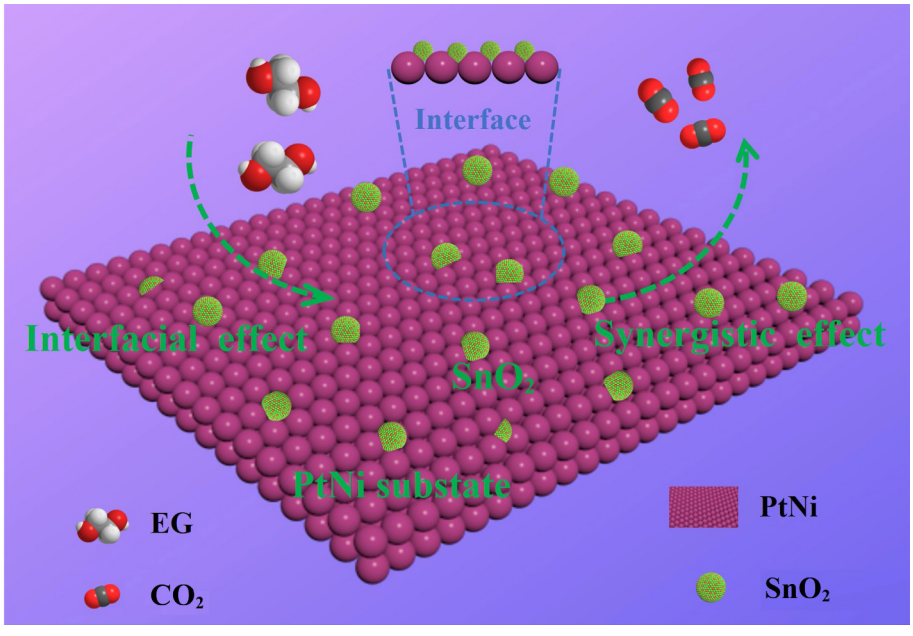

Figure 5 The schematic illustration for enhancement EGOR performance on the interface of SnO_2/PtNi catalyst.

4 Conclusions

In summary, the SnO_2/PtNi catalysts enclosed by HIFs with adjustable SnO_2 composition were designed via integration hydrothermal method with self-assembly approach for high-efficiency EGOR electrocatalysis. The presented SnO_2/PtNi catalysts show the strong interfacial synergistic interactions via electron transfer for drastically boosting electrocatalytic properties. Experimental results have verified that the 0.20%SnO_2/PtNi catalyst displays outstanding electroactivity towards EGOR in comparison with PtNi CNCs and commercial Pt/C catalyst, including exceptional specific/mass activities, excellent long-term durability, and strong resistance to CO toxicity. The kinetic study demonstrates that the interfacial effect between SnO_2 and PtNi can degrade the apparent activation-energy during the process of EGOR. Therefore, the SnO_2/PtNi catalysts integrate undercoordinated active sites and strong interfacial synergistic interaction, which are responsible for the superior catalytic performance towards EGOR. It is expected that this study will afford a potential strategy to design high-efficient electrocatalysts in the future.

Acknowledgements

The authors acknowledge the financial supports from the National Natural Science Foundation of China (No. 21573286) and the Key Scientific and Technological Innovation Project in Shandong Province (No. 2019JZZY010343).

Electronic Supplementary Material: Supplementary material (catalytic results and characterization analysis of these catalysts) is available in the online version of this article at https://doi.org/10.1007/s12274-022-4433-0.

References

[1] Tian, N.; Zhou, Z. Y.; Sun, S. G.; Ding, Y.; Wang, Z. L. Synthesis of tetrahexahedral platinum nanocrystals with high-index facets and high electro-oxidation activity. *Science* **2007**, *316*, 732–735.

[2] Li, M. F.; Zhao, Z. P.; Cheng, T.; Fortunelli, A.; Chen, C. Y.; Yu, R.; Zhang, Q. H.; Gu, L.; Merinov, B. V.; Lin, Z. Y. et al. Ultrafine jagged platinum nanowires enable ultrahigh mass activity for the oxygen reduction reaction. *Science* **2016**, *354*, 1414–1419.

[3] Fu, X. Y.; Wan, C. Z.; Zhang, A. X.; Zhao, Z. P.; Huyan, H. X.; Pan, X. Q.; Du, S. J.; Duan, X. F.; Huang, Y. Pt_3Ag alloy wavy nanowires

as highly effective electrocatalysts for ethanol oxidation reaction. *Nano Res.* **2020**, *13*, 1472–1478.

[4] Du, H. Y.; Wang, K.; Tsiakaras, P.; Shen, P. K. Excavated and dendritic Pt-Co nanocubes as efficient ethylene glycol and glycerol oxidation electrocatalysts. *Appl. Catal. B Environ.* **2019**, *258*, 117951.

[5] Wang, Y.; Zhuo, H. Y.; Sun, H.; Zhang, X.; Dai, X. P.; Luan, C. L.; Qin, C. L.; Zhao, H. H.; Li, J.; Wang, M. L. et al. Implanting Mo atoms into surface lattice of Pt_3Mn alloys enclosed by high-indexed facets: Promoting highly active sites for ethylene glycol oxidation. *ACS Catal.* **2019**, *9*, 442–455.

[6] Niu, Z. Q.; Becknell, N.; Yu, Y.; Kim, D.; Chen, C.; Kornienko, N.; Somorjai, G. A.; Yang, P. D. Anisotropic phase segregation and migration of Pt in nanocrystals enroute to nanoframe catalysts. *Nat. Mater.* **2016**, *15*, 1188–1194.

[7] Erlebacher, J.; Aziz, M. J.; Karma, A.; Dimitrov, N.; Sieradzki, K. Evolution of nanoporosity in dealloying. *Nature* **2001**, *410*, 450–453.

[8] Lu, Q. Q.; Sun, L. T.; Zhao, X.; Huang, J. S.; Han, C.; Yang, X. R. One-pot synthesis of interconnected $Pt_{95}Co_5$ nanowires with enhanced electrocatalytic performance for methanol oxidation reaction. *Nano Res.* **2018**, *11*, 2562–2572.

[9] Zhao, Z. P.; Liu, H. T.; Gao, W. P.; Xue, W.; Liu, Z. Y.; Huang, J.; Pan, X. Q.; Huang, Y. Surface-engineered PtNi-O nanostructure with record-high performance for electrocatalytic hydrogen evolution reaction. *J. Am. Chem. Soc.* **2018**, *140*, 9046–9050.

[10] Yang, J. T.; Ning, G. Q.; Yu, L.; Wang, Y.; Luan, C. L.; Fan, A. X.; Zhang, X.; Liu, Y. J.; Dong, Y.; Dai, X. P. et al. Morphology controllable synthesis of PtNi concave nanocubes enclosed by high-index facets supported on porous graphene for enhanced hydrogen evolution reaction. *J. Mater. Chem. A* **2019**, *7*, 17790–17796.

[11] Wang, Y.; Zhuo, H. Y.; Zhang, X.; Dai, X. P.; Yu, K. M.; Luan, C. L.; Yu, L.; Xiao, Y.; Li, J.; Wang, M. et al. Synergistic effect between undercoordinated platinum atoms and defective nickel hydroxide on enhanced hydrogen evolution reaction in alkaline solution. *Nano Energy* **2018**, *48*, 590–599.

[12] Wang, Y.; Zheng, M.; Li, Y. R.; Ye, C. L.; Chen, J.; Ye, J. Y.; Zhang, Q. H.; Li, J.; Zhou, Z. Y.; Fu, X. Z. et al. p–d orbital hybridization induced by a monodispersed Ga site on a Pt_3Mn nanocatalyst boosts ethanol electrooxidation. *Angew. Chem., Int. Ed.* **2022**, *61*, e202115735.

[13] Rodriguez, J. A.; Liu, P.; Graciani, J.; Senanayake, S. D.; Grinter, D. C.; Stacchiola, D.; Hrbek, J.; Fernández-Sanz, J. Inverse oxide/metal catalysts in fundamental studies and practical applications: A perspective of recent developments. *J. Phys. Chem. Lett.* **2016**, *7*, 2627–2639.

[14] Zhu, Y. F.; Zhang, X.; Koh, K.; Kovarik, L.; Fulton, J. L.; Rosso, K. M.; Gutiérrez, O. Y. Inverse iron oxide/metal catalysts from galvanic replacement. *Nat. Commun.* **2020**, *11*, 3269.

[15] Lyu, Z.; Zhang, X. G.; Wang, Y. C.; Liu, K.; Qiu, C. Y.; Liao, X. Y.; Yang, W. H.; Xie, Z. X.; Xie, S. F. Amplified interfacial effect in an atomically dispersed RuO_x-on-Pd 2D inverse nanocatalyst for high-performance oxygen reduction. *Angew. Chem., Int. Ed.* **2021**, *60*, 16093–16100.

[16] Wang, L.; Wu, W.; Lei, Z.; Zeng, T.; Tan, Y. Y.; Cheng, N. C.; Sun, X. L. High-performance alcohol electrooxidation on Pt_3Sn-SnO_2 nanocatalysts synthesized through the transformation of Pt-Sn nanoparticles. *J. Mater. Chem. A* **2020**, *8*, 592–598.

[17] Wang, H.; Liu, Z. Y.; Ma, Y. J.; Julian, K.; Ji, S.; Linkov, V.; Wang, R. F. Synthesis of carbon-supported PdSn-SnO_2 nanoparticles with different degrees of interfacial contact and enhanced catalytic activities for formic acid oxidation. *Phys. Chem. Chem. Phys.* **2013**, *15*, 13999–14005.

[18] Shen, X. C.; Nagai, T.; Yang, F. P.; Zhou, L. Q.; Pan, Y. B.; Yao, L. B.; Wu, D. Z.; Liu, Y. S.; Feng, J.; Guo, J. H. et al. Dual-site cascade oxygen reduction mechanism on SnO_x/Pt-Cu-Ni for promoting reaction kinetics. *J. Am. Chem. Soc.* **2019**, *141*, 9463–9467.

[19] Luan, C. L.; Zhou, Q. X.; Wang, Y.; Xiao, Y.; Dai X. P.; Huang X. L.; Zhang X. A general strategy assisted with dual reductants and dual protecting agents for preparing Pt-based alloys with high-index facets and excellent electrocatalytic performance. *Small* **2017**, *13*, 1702617.

[20] Li, Y. R.; Wang, Y.; Li, S. N.; Li, M. X.; Liu, Y. J.; Fang, X.; Dai, X. P.; Zhang, X. Pt_3Mn alloy nanostructure with high-index facets by Sn doping modified for highly catalytic active electro-oxidation reactions. *J. Catal.* **2021**, *395*, 282–292.

[21] Huang, H. J.; Wei, Y. J.; Yang, Y.; Yan, M. M.; He, H. Y.; Jiang, Q. G.; Yang, X. F.; Zhu, J. X. Controllable synthesis of grain boundary-enriched Pt nanoworms decorated on graphitic carbon nanosheets for ultrahigh methanol oxidation catalytic activity. *J. Energy Chem.* **2021**, *57*, 601–609.

[22] Kim, C.; Noh, M.; Choi, M.; Cho, J.; Park, B. Critical size of a nano SnO_2 electrode for Li-secondary battery. *Chem. Mater.* **2005**, *17*, 3297–3301.

[23] Wang, K. L.; Wang, F.; Zhao, Y. F.; Zhang, W. Q. Surface-tailored PtPdCu ultrathin nanowires as advanced electrocatalysts for ethanol oxidation and oxygen reduction reaction in direct ethanol fuel cell. *J. Energy Chem.* **2021**, *52*, 251–261.

[24] Gruzeł, G.; Piekarz, P.; Pawlyta, M.; Donten, M.; Parlinska-Wojtan, M. Preparation of Pt-skin PtRhNi nanoframes decorated with small SnO_2 nanoparticles as an efficient catalyst for ethanol oxidation reaction. *ACS Appl. Mater. Interfaces* **2019**, *11*, 22352–22363.

[25] Guan, J. Y.; Zan, Y. X.; Shao, R.; Niu, J.; Dou, M. L.; Zhu, B. N.; Zhang, Z. P.; Wang, F. Phase segregated Pt-SnO_2/C nanohybrids for highly efficient oxygen reduction electrocatalysis. *Small* **2020**, *16*, 2005048.

[26] Zhu, L. H.; Zhu, H. Z.; Shakouri, M.; Zeng, L. H.; Yang, Z. Q.; Hu, Y. F.; Ye, H. Q.; Wang, H.; Chen, B. H.; Luque, R. Mechanistic insights into interfacial nano-synergistic effects in trimetallic Rh-on-NiCo on-CNTs for room temperature solvent-free hydrogenations. *Appl. Catal. B Environ.* **2021**, *297*, 120404.

[27] Yu, L.; Zhou, T. T.; Cao, S. H.; Tai, X. S.; Liu, L. L.; Wang, Y. Suppressing the surface passivation of Pt-Mo nanowires via constructing Mo-Se coordination for boosting HER performance. *Nano Res.* **2021**, *14*, 2659–2665.

[28] Song, D. Y.; Wang, S. S.; Liu, R. Z.; Jiang, J. L.; Jiang, Y.; Huang, S. S.; Li, W. R.; Chen, Z. W.; Zhao, B. Ultra-small SnO_2 nanoparticles decorated on three-dimensional nitrogen-doped graphene aerogel for high-performance bind-free anode material. *Appl. Surf. Sci.* **2019**, *478*, 290–298.

[29] Wang, Y.; Zheng, X. E.; Wang, D. S. Design concept for electrocatalysts. *Nano Res.* **2022**, *15*, 1730–1752.

[30] Nagasawa, K.; Takao, S.; Nagamatsu, S. I.; Samjeské, G.; Sekizawa, O.; Kaneko, T.; Higashi, K.; Yamamoto, T.; Uruga, T.; Iwasawa, Y. Surface-regulated nano-SnO_2/Pt_3Co/C cathode catalysts for polymer electrolyte fuel cells fabricated by a selective electrochemical Sn deposition method. *J. Am. Chem. Soc.* **2015**, *137*, 12856–12864.

[31] Gao, Q.; Mou, T. Y.; Liu, S. K.; Johnson, G.; Han, X.; Yan, Z. H.; Ji, M. X.; He, Q.; Zhang, S.; Xin, H. L. et al. Monodisperse PdSn/SnO_x core/shell nanoparticles with superior electrocatalytic ethanol oxidation performance. *J. Mater. Chem. A* **2020**, *8*, 20931–20938.

[32] Liu, M. M.; Tang, W. Q.; Xie, Z. H.; Yu, H. B.; Yin, H. F.; Xu, Y. S.; Zhao, S. L.; Zhou, S. H. Design of highly efficient Pt-SnO_2 hydrogenation nanocatalysts using Pt@Sn core–shell nanoparticles. *ACS Catal.* **2017**, *7*, 1583–1591.

[33] Zhang, H.; Du, N.; Chen, B. D.; Cui, T. F.; Yang, D. R. Sub-2 nm SnO_2 nanocrystals: A reduction/oxidation chemical reaction synthesis and optical properties. *Mater. Res. Bull.* **2008**, *43*, 3164–3170.

[34] Sun, L.; Wang, B.; Wang, Y. D. High-temperature gas sensor based on novel Pt single atoms@SnO_2 nanorods@SiC nanosheets multi-heterojunctions. *ACS Appl. Mater. Interfaces* **2020**, *12*, 21808–21817.

[35] Li, Z. X.; Wang, R.; Xue, J. J.; Xing, X. F.; Yu, C. C.; Huang, T. Y.; Chu, J. M.; Wang, K. L.; Dong, C.; Wei, Z. T. et al. Core–shell ZnO@SnO_2 nanoparticles for efficient inorganic perovskite solar cells. *J. Am. Chem. Soc.* **2019**, *141*, 17610–17616.

[36] Jiang, L. H.; Sun, G. Q.; Zhou, Z. H.; Zhou, W. J.; Xin, Q. Preparation and characterization of PtSn/C anode electrocatalysts for direct ethanol fuel cell. *Catal. Today* **2004**, *93–95*, 665–670.

[37] Zheng, J. N.; Lv, J. J.; Li, S. S.; Xue, M. W.; Wang, A. J.; Feng, J. J. One-pot synthesis of reduced graphene oxide supported hollow

Ag@Pt core–shell nanospheres with enhanced electrocatalytic activity for ethylene glycol oxidation. *J. Mater. Chem. A* **2014**, *2*, 3445.

[38] Zhang, N.; Bu, L. Z.; Guo, S. J.; Guo, J.; Huang, X. Q. Screw thread-like platinum-copper nanowires bounded with high-index facets for efficient electrocatalysis. *Nano Lett.* **2016**, *16*, 5037–5043.

[39] Chen, H. S.; Benedetti, T. M.; Lian, J. X.; Cheong, S.; O'Mara, P. B.; Sulaiman, K. O.; Kelly, C. H. W.; Scott, R. W. J.; Gooding, J. J.; Tilley, R. D. Role of the secondary metal in ordered and disordered Pt-M intermetallic nanoparticles: An example of Pt_3Sn nanocubes for the electrocatalytic methanol oxidation. *ACS Catal.* **2021**, *11*, 2235–2243.

[40] Zhu, J. Y.; Chen, S. Q.; Xue, Q.; Li, F. M.; Yao, H. C.; Xu, L.; Chen, Y. Hierarchical porous Rh nanosheets for methanol oxidation reaction. *Appl. Catal. B Environ.* **2020**, *264*, 118520.

[41] Zhang, Z. C.; Luo, Z. M.; Chen, B.; Wei, C.; Zhao, J.; Chen, J. Z.; Zhang, X.; Lai, Z. C.; Fan, Z. X.; Tan, C. L. et al. One-pot synthesis of highly anisotropic five-fold-twinned PtCu nanoframes used as a bifunctional electrocatalyst for oxygen reduction and methanol oxidation. *Adv. Mater.* **2016**, *28*, 8712–8717.

[42] Zhang, N.; Li, X. Y.; Ye, H. C.; Chen, S. M.; Ju, H. X.; Liu, D. B.; Lin, Y.; Ye, W.; Wang, C. M.; Xu, Q. et al. Oxide defect engineering enables to couple solar energy into oxygen activation. *J. Am. Chem. Soc.* **2016**, *138*, 8928–8935.

[43] Xu, G. R.; Wang, B.; Zhu, J. Y.; Liu, F. Y.; Chen, Y.; Zeng, J. H.; Jiang, J. X.; Liu, Z. H.; Tang, Y. W.; Lee, J. M. Morphological and interfacial control of platinum nanostructures for electrocatalytic oxygen reduction. *ACS Catal.* **2016**, *6*, 5260–5267.

[44] Wang, Y.; Wang, D. S.; Li, Y. D. A fundamental comprehension and recent progress in advanced Pt-based ORR nanocatalysts. *SmartMat* **2021**, *2*, 56–75.

[45] Fan, X. K.; Tang, M.; Wu, X. T.; Luo, S. P.; Chen, W.; Song, X.; Quan, Z. W. SnO_2 patched ultrathin PtRh nanowires as efficient catalysts for ethanol electrooxidation. *J. Mater. Chem. A* **2019**, *7*, 27377–27382.

[46] Li, R. H.; Liu, Z. Q.; Trinh, Q. T.; Miao, Z. Q.; Chen, S.; Qian, K. C.; Wong, R. J.; Xi, S. B.; Yan, Y.; Borgna, A. et al. Strong metal–support interaction for 2D materials: Application in noble metal/TiB_2 heterointerfaces and their enhanced catalytic performance for formic acid dehydrogenation. *Adv. Mater.* **2021**, *33*, 2101536.

[47] Kowal, A.; Li, M.; Shao, M.; Sasaki, K.; Vukmirovic, M. B.; Zhang, J.; Marinkovic, N. S.; Liu, P.; Frenkel, A. I.; Adzic, R. R. Ternary Pt/Rh/SnO_2 electrocatalysts for oxidizing ethanol to CO_2. *Nat. Mater.* **2009**, *8*, 325–330.

[48] Du, W. X.; Yang, G. X.; Wong, E.; Deskins, N. A.; Frenkel, A. I.; Su, D.; Teng, X. W. Platinum-tin oxide core–shell catalysts for efficient electro-oxidation of ethanol. *J. Am. Chem. Soc.* **2014**, *136*, 10862–10865.

[49] Li, M.; Cullen, D. A.; Sasaki, K.; Marinkovic, N. S.; More, K.; Adzic, R. R. Ternary electrocatalysts for oxidizing ethanol to carbon dioxide: Making Ir capable of splitting C–C bond. *J. Am. Chem. Soc.* **2013**, *135*, 132–141.

[50] Rizo, R.; Bergmann, A.; Timoshenko, J.; Scholten, F.; Rettenmaier, C.; Jeon, H. S.; Chen, Y. T.; Yoon, A.; Bagger, A.; Rossmeisl, J. et al. Pt-Sn-Co nanocubes as highly active catalysts for ethanol electro-oxidation. *J. Catal.* **2021**, *393*, 247–258.

[51] Kim, H. J.; Choi, S. M.; Green, S.; Tompsett, G. A.; Lee, S. H.; Huber, G. W.; Kim, W. B. Highly active and stable PtRuSn/C catalyst for electrooxidations of ethylene glycol and glycerol. *Appl. Catal. B Environ.* **2011**, *101*, 366–375.

[52] Serov, A.; Kwak, C. Recent achievements in direct ethylene glycol fuel cells (DEGFC). *Appl. Catal. B Environ.* **2010**, *97*, 1–12.

[53] Tang, J. X.; Xiao, L. P.; Xiao, C.; Tian, N.; Zhou, Z. Y.; Sun, S. G. Tetrahexahedral PdRh nanocrystals with tunable composition as a highly efficient electrocatalyst for ethylene glycol oxidation. *J. Mater. Chem. A* **2021**, *9*, 11049–11055.

[54] Lin, J. L.; Ren, J.; Tian, N.; Zhou, Z. Y.; Sun, S. G. *In situ* FTIR spectroscopic studies of ethylene glycol electrooxidation on Pd electrode in alkaline solution: The effects of concentration. *J. Electroanal. Chem.* **2013**, *688*, 165–171.

[55] Krittayavathananon, A.; Sawangphruk, M. Electrocatalytic oxidation of ethylene glycol on palladium coated on 3D reduced graphene oxide aerogel paper in alkali media: Effects of carbon supports and hydrodynamic diffusion. *Electrochim. Acta* **2016**, *212*, 237–246.

[56] Ferrin, P.; Mavrikakis, M. Structure sensitivity of methanol electrooxidation on transition metals. *J. Am. Chem. Soc.* **2009**, *131*, 14381–14389.

[57] Liu, G. G.; Zhou, W.; Ji, Y. R.; Chen, B.; Fu, G. T.; Yun, Q. B.; Chen, S. M.; Lin, Y. X.; Yin, P. F.; Cui, X. Y. et al. Hydrogen-intercalation-induced lattice expansion of Pd@Pt core–shell nanoparticles for highly efficient electrocatalytic alcohol oxidation. *J. Am. Chem. Soc.* **2021**, *143*, 11262–11270.